Bayesian Experimental Design of Cyber-Physical Tests for Hydrodynamic Model Calibration

G. Abbiati*[1] and T. Sauder†[2]

[1]*Department of Civil and Architectural Engineering, Aarhus University, Denmark*
[2]*SINTEF Ocean AS, Norwegian University of Science and Technology, Trondheim, Norway*

Draft submitted to *engrXiv*

March 9, 2021

Abstract

An application of cyber-physical testing to the empirical estimation of difference-frequency quadratic transfer functions is presented. As an alternative to today's procedure based on hydrodynamic tests with broad-banded or realistic (e.g., JONSWAP) wave spectra, tests in bichromatic waves are considered. The laboratory setup is the one developed by Sauder & Tahchiev (2020) that enables magnifying the sensitivity of the floater response to the low-frequency wave loading by adjusting the stiffness and damping parameters of a virtual soft mooring system. Bayesian experimental design is proposed to optimize the selection of the control variables (frequencies in the bichromatic wave and properties of the virtual mooring system) for a batch of cyber-physical tests. The experimental design algorithm is based on the recent work of Huan & Marzouk (2013). In a virtual yet realistic case study using an uncertain parametric quadratic transfer function, we demonstrate how the uncertainty of its describing parameters and other calibration parameters (low-frequency added mass and hydrodynamic damping) can be reduced. Results indicate that the proposed procedure has the potential for reducing experimental cost for calibration of hydrodynamic models.

Keywords: Hydrodynamic testing; cyber-physical testing; Bayesian experimental design; model calibration; quadratic transfer function.

1 INTRODUCTION

1.1 Background and motivation

The design of moored floating structures requires validated computational models to predict wave-frequency (WF) and low-frequency (LF) hydrodynamic loads [1]. In general, first-order potential flow theory provides sufficiently accurate estimates of WF loads when viscous effects are negligible. LF loads, which are crucial for determining extreme offsets and tension in mooring lines, are generally described by Quadratic Transfer Function (QTF) that represent the relationship between the amplitudes of two monochromatic waves of frequencies $\{f_1, f_2\}$, and the LF load exerted to the floater at a frequency $|f_1 - f_2|$. See the previous reference for details. An example of QTF is shown in Figure 1 for a ship-shaped floating structure in head seas.

QTFs obtained with numerical tools accurately predict LF loads in mild sea states and in the absence of current. However, since the existing numerical methods are based on potential theory, perturbation methods, and treat the presence of current only through approximations, they generally fail at predicting LF loads accurately in moderate-to-extreme sea states where current effects, viscous effects, and beyond-second-order potential effects become significant.

Therefore, empirical methods play a central role in improving such QTF estimates [2]. As of today, state-of-the-art model-tests practice is to install the offshore structure under study in an ocean basin, using a so-called *soft mooring system*. The stiffness of the mooring system in surge, sway and yaw is fixed and designed to be low, leading to natural periods well above the WF range. This in order not to disturb the WF motions of the

*Dr. Giuseppe Abbiati, `abbiati@cae.au.dk`, ORCID: `0000-0002-5048-8505`.
†Dr. Thomas Sauder, `thomas.sauder@sintef.no`, ORCID: `0000-0001-7445-7239`.

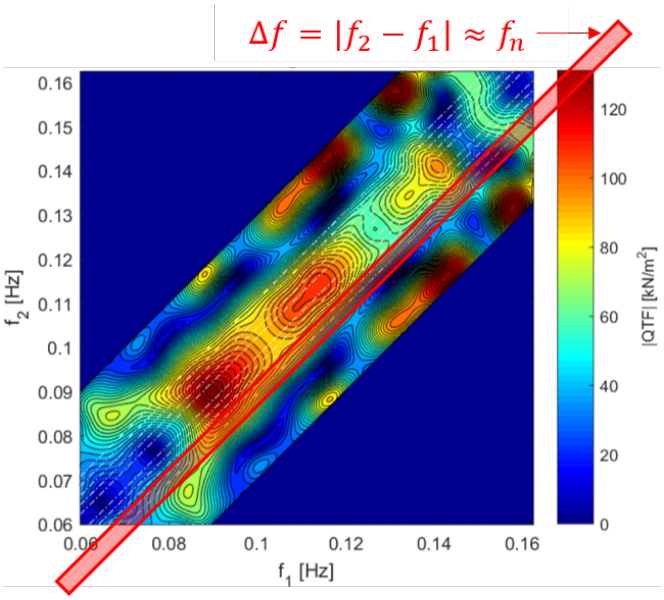

Figure 1: Example of QTF amplitude: the red box indicates the domain of wave frequency pairs $\{f_1, f_2\}$ leading to a LF excitation with frequency $\Delta f = f_1 - f_2$ tuned with the floater eigenfrequency f_n.

floater, which play an important role for the LF wave loads. The system is then subjected to incoming waves representing either a realistic sea-state (wave energy concentrated around a peak period) or a broad-banded wave spectrum. Based on input wave amplitude and floater motion, a linear deconvolution and cross-bi-spectral analysis are performed to compute a non-parametric estimate of the QTF for the net LF wave load exerted to the floater [3]. Besides the statistical uncertainty inherent to this type of estimation, two main limitations can be mentioned: i) when LF wave loads and floater transfer function are detuned (i.e. the oscillator does not respond significantly to the wave load at the studied frequency), no information on LF load is present on the floater response and, therefore, deconvolution is not applicable; ii) the accurate identification of the QTF requires that *significant* wave energy is allocated for any frequency pair $\{f_1, f_2\}$, which is difficult to achieve in practice for sufficiently broad range of frequency pairs.

In response to the first limitation, Sauder & Tahchiev [4] developed a laboratory apparatus that enables magnifying the sensitivity of the floater response to the LF loads generated by the incoming wave by adjusting the stiffness and damping parameters of a *virtual* soft mooring system. This type of *Cyber-Physical* (CP) testing method has been introduced earlier in hydrodynamic testing, under the denomination Real-time Hybrid Model testing*[5]. A CP model comprises a physical subsystem tested in the laboratory, and a numerical subsystem simulated numerically. The two subsystems interact with each other in a closed-loop as parts of a unique prototype. In hydrodynamic testing, the physical subsystem (the floater) is installed in an ocean basin, and boundary conditions computed from the numerical subsystem (the virtual mooring) are prescribed using a real-time control system. Here, CP testing is performed in force-control, that is, a set of actuation lines impose the virtual mooring forces to the floater, and the corresponding LF velocity and position feedback close the simulation loop. More details can be found in Section 4.1 and in [4].

In response to the second limitation, one could perform a sufficiently large number of CP tests based on bichromatic waves to cover the entire domain of the QTF $\{f_1, f_2\}$ with a sufficiently dense grid. However, it requires about $30 - 40$ min to complete a single experiment before starting a new one; therefore, a brutal mapping of the QTF is not feasible due to time constraints.

1.2 Scope

Instead of scanning the whole grid of frequency pairs systematically to compute a non-parametric estimate of the QTF, this paper proposes to calibrate a parametrized QTF model based on a minimal set of CP tests. Bayesian Experimental Design (Bayesian-ED) is proposed to optimize the selection of the control variables for an entire batch of CP tests so that the expected reduction of uncertainty of the QTF calibration parameters is maximized. Noteworthy such control variables include both the frequencies of bi-chromatic waves and stiffness and damping of the active mooring system. As a result, the floater transfer function can be tuned to the incoming LF wave load (limitation i)) and the entire domain of the QTF can be explored (limitation ii)).

*ReaTHM® testing is a registered trademark of SINTEF Ocean.

Model calibration is a cornerstone of engineering science provided with a mathematically sound framework rooted in Bayesian inference [6, 7]. In principle, a forward model, some experimental observation, and a measure of their likelihood are used to infer some quantity of interest not directly observable (i.e., calibration parameters). A set of control variables determines the experimental conditions from which observations are taken. Bayesian-ED provides a decision-theoretic methodology to optimize the selection of such control variables [8, 9]. Since the outcome of an experiment is uncertain, Bayesian-ED is performed by maximizing the *expected* value of a utility function. The latter is usually expressed in terms of a measure of the information gain on calibration parameters following the experiment.

In this work, the Bayesian-ED algorithm presented in a recent work of Huan & Marzouk [10] is adopted to design a batch of CP tests. The selected utility function is defined as the Kullback-Leibler divergence [11] from prior to posterior probability density functions (PDF) of calibration parameters. The effectiveness of the proposed approach is demonstrated for a virtual hydrodynamic application where a QTF model is calibrated. In this example, the QTF model consists of a mixture of bivariate Gaussian functions [11].

The paper is organized as follows. Section 2 provides the basics of Bayesian model calibration. The aim is to introduce the fundamental terminology and to provide a self-contained mathematical notation. Section 3 describes the Bayesian-ED procedure introduced by Huan & Marzouk [10] and utilized in this work. Section 4 presents the application example. CP testing is used to calibrate the parameters of the QTF for a typical moored system. Main conclusions are summarized in Section 5.

2 BAYESIAN MODEL CALIBRATION

This section recalls the basics of Bayesian calibration of computer models in its simplest form, that is, for the case of a deterministic computational model and statistically independent observations. The aim is to provide a self-contained notation for the proposed Bayesian-ED procedure, which is described in the next section. For a more generic treatment of the Bayesian calibration problem and a comprehensive review of the state of the art, the reader is addressed to the work of Nagel & Sudret [7].

The relationship between an observation $\mathbf{y}_i \in \mathcal{D}_\mathbf{y} \subset \mathbb{R}^{n_y}$ and the corresponding forward model prediction $\boldsymbol{\mathcal{M}}(\boldsymbol{\theta}, \mathbf{d}_i)$ reads,

$$\mathbf{y}_i = \boldsymbol{\mathcal{M}}(\boldsymbol{\theta}, \mathbf{d}_i) + \boldsymbol{\epsilon}_i \tag{1}$$

where the index $i \in \{1, \dots, n\}$ indicates a specific experiment of a batch. $\boldsymbol{\theta} \in \mathcal{D}_{\boldsymbol{\theta}} \subset \mathbb{R}^{n_\theta}$ are deterministic albeit unknown *calibration parameters* and, therefore, associated with epistemic uncertainty. Accordingly, calibration parameters are thought as of a realization a *prior* probability density function (PDF) $\boldsymbol{\theta} \sim \pi(\boldsymbol{\theta})$, which reflects prior belief on possible values. $\mathbf{d}_i \in \mathcal{D}_\mathbf{d} \subset \mathbb{R}^{n_d}$ comprises all those variables that can be controlled by the experiments and therefore indicated as *control variables*. Finally, the discrepancy term $\boldsymbol{\epsilon}_i \in \mathcal{D}_{\boldsymbol{\epsilon}} \subset \mathbb{R}^{n_y}$ incorporates model inadequacies and measurement errors. Commonly, the residual term is assumed as of a realization of a normal distributions $\boldsymbol{\epsilon}_i \sim \mathcal{N}(\mathbf{0}, \boldsymbol{\Sigma}_i)$ with zero mean and experiment-specific symmetric positive-semidefinite covariance matrix $\boldsymbol{\Sigma}_i$. The set of all available experimental observations $\boldsymbol{\mathcal{Y}} = \{\mathbf{y}_1 \dots \mathbf{y}_i \dots \mathbf{y}_n\}$ and the corresponding samples of control variables $\boldsymbol{\mathcal{D}} = \{\mathbf{d}_1 \dots \mathbf{d}_i \dots \mathbf{d}_n\}$ form the so-called Experimental Design (ED) $\{\boldsymbol{\mathcal{D}}, \boldsymbol{\mathcal{Y}}\}$ for the Bayesian calibration problem.

In this paper, (1) refers to a single CP test of a batch of n CP tests. The forward model $\mathcal{M}(\boldsymbol{\theta}, \mathbf{d}_i)$ includes a computational model of the PS of parameters $\boldsymbol{\theta}$. The remaining known parameters of the CP model are stored in $\mathbf{d}_i$. For the sake of simplicity, both NS, PS and external loading models and therefore $\mathcal{M}(\boldsymbol{\theta}, \mathbf{d}_i)$ are assumed as deterministic.

Given a forward model in the format specified in (1), an ED acquired from a batch of n experiments, a probabilistic model for discrepancy and the prior PDFs of calibration parameters, the Bayes' rule for conditional probability is used to compute the posterior PDF of calibration parameters,

$$\pi(\boldsymbol{\theta}|\boldsymbol{\mathcal{D}}, \boldsymbol{\mathcal{Y}}) = \frac{\mathcal{L}(\boldsymbol{\theta}; \boldsymbol{\mathcal{D}}, \boldsymbol{\mathcal{Y}})\pi(\boldsymbol{\theta})}{\pi(\boldsymbol{\mathcal{Y}}|\boldsymbol{\mathcal{D}})} \tag{2}$$

where the *likelihood* function $\mathcal{L}(\boldsymbol{\theta}; \boldsymbol{\mathcal{D}}, \boldsymbol{\mathcal{Y}})$ measures the evidence of $\boldsymbol{\theta}$ provided by the ED. For simplicity, in this paper, experimental observations are assumed as statistically independent. Still, for simplicity, discrepancy terms are assumed as uncorrelated between different forward model outputs. Therefore, $\boldsymbol{\Sigma}_i$ is diagonal. The expression of the likelihood term of (2) reads,

$$\mathcal{L}(\boldsymbol{\theta};\boldsymbol{\mathcal{D}},\boldsymbol{\mathcal{Y}}) = \prod_{i=1}^{n} \frac{1}{\sqrt{(2\pi)^{n_y}\det(\boldsymbol{\Sigma}_i)}} \exp -\frac{1}{2}\left[(\mathbf{y}_i - \mathcal{M}(\boldsymbol{\theta},\mathbf{d}_i))\,\boldsymbol{\Sigma}_i^{-1}\,(\mathbf{y}_i - \mathcal{M}(\boldsymbol{\theta},\mathbf{d}_i))^{\top}\right] \tag{3}$$

The denominator of the right-hand side of (2) is called *marginal likelihood* or *evidence* and it is obtained by applying the total probability theorem,

$$\pi(\boldsymbol{\mathcal{Y}}|\boldsymbol{\mathcal{D}}) = \int_{\mathcal{D}_{\boldsymbol{\theta}}} \mathcal{L}(\boldsymbol{\theta};\boldsymbol{\mathcal{D}},\boldsymbol{\mathcal{Y}})\pi(\boldsymbol{\theta})d\boldsymbol{\theta} \tag{4}$$

The solution of (4) is typically avoided and the unnormalized posterior PDF of $\boldsymbol{\theta}$ is sampled numerically using Markov Chain Monte Carlo (MCMC) methods.

3 BAYESIAN EXPERIMENTAL DESIGN

This section describes the Bayesian-ED procedure proposed by Huan & Marzouk [10] and its application to CP testing. This combination is the essence of the novelty carried by this paper.

3.1 Theoretical derivation of the utility function

The Bayesian-ED procedure proposed by Huan & Marzouk [10] follows the decision-theoretic approach as originally introduced by Lindley [12]. The review paper of Chaloner & Verdinelli provides a comprehensive overview on this subject [8]. In a decision-theoretic approach, an utility function $u(\boldsymbol{\mathcal{Y}},\boldsymbol{\mathcal{D}})$ quantifies the information gain provided by a specific ED. The utility function reflects the goal of the experimental campaign. Noteworthy, for a given $\boldsymbol{\mathcal{D}}$, experimental observations collected in $\boldsymbol{\mathcal{Y}}$ propagates the uncertainties of calibration parameters $\boldsymbol{\theta}$ and model discrepancy $\boldsymbol{\epsilon}$. Accordingly, $u(\boldsymbol{\mathcal{Y}},\boldsymbol{\mathcal{D}})$ is also uncertain. Therefore, Bayesian optimal ED is performed with respect to the expected value of the utility function,

$$U(\boldsymbol{\mathcal{D}}) = \int_{\mathcal{D}_{\boldsymbol{\mathcal{Y}}}} u(\boldsymbol{\mathcal{Y}},\boldsymbol{\mathcal{D}})\pi(\boldsymbol{\mathcal{Y}}|\boldsymbol{\mathcal{D}})d\boldsymbol{\mathcal{Y}} \tag{5}$$

where $\pi(\boldsymbol{\mathcal{Y}}|\boldsymbol{\mathcal{D}})$ represents the probability measure associated with a specific ED $\{\boldsymbol{\mathcal{D}},\boldsymbol{\mathcal{Y}}\}$. It is clear from (4) that the averaging of (5) adds less weight to those EDs for which experimental observations $\boldsymbol{\mathcal{Y}}$ are unlikely either because corresponding calibration parameters are unlikely (small prior $\pi(\boldsymbol{\theta})$) or discrepancy is unlikely (small likelihood $\mathcal{L}(\boldsymbol{\theta};\boldsymbol{\mathcal{D}},\boldsymbol{\mathcal{Y}})$). The solution of the Bayesian-ED problem reduces to the following maximization problem,

$$\hat{\boldsymbol{\mathcal{D}}} = \arg\max_{\boldsymbol{\mathcal{D}}} U(\boldsymbol{\mathcal{D}}) \tag{6}$$

For the specific case where experimental observations are used to calibrate the parameters of a computational model (see Section 2), Huan & Marzouk [10] proposed to adopt as utility function the Kullback–Leibler (KL) divergence [11], a.k.a. relative entropy, from the posterior to the prior PDF of calibration parameters,

$$\begin{aligned} u(\boldsymbol{\mathcal{Y}},\boldsymbol{\mathcal{D}}) &= D_{KL}(\pi(\boldsymbol{\theta}|\boldsymbol{\mathcal{Y}},\boldsymbol{\mathcal{D}})||\pi(\boldsymbol{\theta})) \\ &= \int_{\mathcal{D}_{\boldsymbol{\theta}}} \pi(\boldsymbol{\theta}|\boldsymbol{\mathcal{Y}},\boldsymbol{\mathcal{D}}) \ln\left[\frac{\pi(\boldsymbol{\theta}|\boldsymbol{\mathcal{Y}},\boldsymbol{\mathcal{D}})}{\pi(\boldsymbol{\theta})}\right] d\boldsymbol{\theta} \end{aligned} \tag{7}$$

The intuition behind (7) is that a large D_{KL} divergence from posterior to prior implies that the data in $\boldsymbol{\mathcal{Y}}$ decreases the entropy in $\boldsymbol{\theta}$ and hence this data is more informative. The expression for the expected utility is obtained by substituting (7) in (5),

$$U(\boldsymbol{\mathcal{D}}) = \int_{\mathcal{D}_{\boldsymbol{\mathcal{Y}}}} \int_{\mathcal{D}_{\boldsymbol{\theta}}} \pi(\boldsymbol{\theta}|\boldsymbol{\mathcal{Y}},\boldsymbol{\mathcal{D}}) \ln\left[\frac{\pi(\boldsymbol{\theta}|\boldsymbol{\mathcal{Y}},\boldsymbol{\mathcal{D}})}{\pi(\boldsymbol{\theta})}\right] \pi(\boldsymbol{\mathcal{Y}}|\boldsymbol{\mathcal{D}})d\boldsymbol{\theta}d\boldsymbol{\mathcal{Y}} \tag{8}$$

Still in [10], it is demonstrated that (8) is equivalent to the mutual information between $\boldsymbol{\theta}$ and $\boldsymbol{\mathcal{Y}}$. Mutual information is a measure of the mutual dependence between two random variables [11].

3.2 Numerical computation of the expected utility

In general, there are no analytical solutions for computing the expected utility function, so the integral of (5) is solved numerically using Monte Carlo. According to the procedure described in [10], with few manipulations (which are omitted for brevity), the expected utility of (5) is rearranged as follows,

$$U(\boldsymbol{\mathcal{D}}) = \int_{\mathcal{D}_{\boldsymbol{\mathcal{Y}}}} \int_{\mathcal{D}_{\boldsymbol{\theta}}} [\ln \pi(\boldsymbol{\mathcal{Y}}|\boldsymbol{\theta}, \boldsymbol{\mathcal{D}}) - \ln \pi(\boldsymbol{\mathcal{Y}}|\boldsymbol{\mathcal{D}})] \\ \pi(\boldsymbol{\mathcal{Y}}|\boldsymbol{\theta}, \boldsymbol{\mathcal{D}})\pi(\boldsymbol{\theta}) d\boldsymbol{\theta} d\boldsymbol{\mathcal{Y}} \tag{9}$$

Then, (9) is evaluated using two nested Monte Carlo loops. Specifically, the outer Monte Carlo loop evaluates the expected utility function,

$$U(\boldsymbol{\mathcal{D}}) \approx \frac{1}{n_{MC,out}} \sum_{j=1}^{n_{MC,out}} \ln \pi(\boldsymbol{\mathcal{Y}}_j|\boldsymbol{\theta}_j, \boldsymbol{\mathcal{D}}) - \ln \pi(\boldsymbol{\mathcal{Y}}_j|\boldsymbol{\mathcal{D}}) \tag{10}$$

where $\boldsymbol{\mathcal{Y}}_j \sim \pi(\boldsymbol{\mathcal{Y}}|\boldsymbol{\theta}, \boldsymbol{\mathcal{D}})$ and $\boldsymbol{\theta}_j \sim \pi(\boldsymbol{\theta})$. The inner Monte Carlo loop computes the marginal likelihood of the ED $\{\boldsymbol{\mathcal{D}}, \boldsymbol{\mathcal{Y}}_j\}$ in (10),

$$\pi(\boldsymbol{\mathcal{Y}}_j|\boldsymbol{\mathcal{D}}) \approx \frac{1}{n_{MC,in}} \sum_{k=1}^{n_{MC,in}} \pi(\boldsymbol{\mathcal{Y}}_j|\boldsymbol{\theta}_k, \boldsymbol{\mathcal{D}}) \tag{11}$$

where $\boldsymbol{\theta}_k \sim \pi(\boldsymbol{\theta})$. Sampling and evaluating the likelihood terms of (10) and (11) entail the evaluation of the forward model. Therefore, they are the most computationally expensive tasks in the calculation of the expected utility function. Accordingly, for a given value of $\boldsymbol{\mathcal{D}}$, the same fresh batch of $\boldsymbol{\theta}_j$ is used as $\boldsymbol{\theta}_k$ ($n_{MC,out} = n_{MC,in} = n_{MC}$) and corresponding—deterministic—forward model evaluations $\mathcal{M}(\boldsymbol{\theta}_j, \mathbf{d}_i), \mathbf{d}_i \in \boldsymbol{\mathcal{D}}$ are stored. Observations ($\boldsymbol{\mathcal{Y}}_j$) and corresponding likelihoods ($\pi(\boldsymbol{\mathcal{Y}}_j|\boldsymbol{\theta}_j, \boldsymbol{\mathcal{D}})$ in (10) and $\pi(\boldsymbol{\mathcal{Y}}_j|\boldsymbol{\theta}_k, \boldsymbol{\mathcal{D}})$ in (11)) are obtained by sampling and evaluating the joint PDF of the the discrepancy term. As a result, the cost for computing (8) is reduced from $n_{MC,out} \times n_{MC,in}$ to n_{MC} evaluations of the forward model. As highlighted in [10], this approach leads to a biased estimator of the expected utility. However, the bias is small.

4 APPLICATION EXAMPLE

In order to exemplify the presented Bayesian-ED procedure for the calibration of QTFs, the following virtual cyber-physical testing campaign is conceived.

4.1 Description of the case study

The objective is to identify empirically a QTF defined on a relevant range of mean frequencies $f_0 = (f_1 + f_2)/2$ and difference-frequencies $\Delta f = f_1 - f_2$ (note that Δf is the frequency of the loading). For simplicity, mimicking the patterns that can be seen on a realistic QTFs such as in Figure 1, we assume that Q is represented analytically by a real multivariate Gaussian mixture model with three lobes (see Figure 3), namely lobe a, b and c:

$$Q(\boldsymbol{\theta}_F, \Delta f, f_0) = Q_a + Q_b + Q_c \tag{12}$$

where,

$$Q_a = A_a \exp\left[\frac{(f_1 - f_a)^2}{2\sigma_a^2} - \frac{(f_2 - f_a)^2}{2\sigma_a^2}\right] \tag{13}$$

$$Q_b = A_b \exp\left[\frac{(f_1 - f_{b_1})^2}{2\sigma_{b_1}^2} - \frac{(f_2 - f_{b_2})^2}{2\sigma_{b_2}^2}\right] + \\ A_b \exp\left[\frac{(f_1 - f_{b_2})^2}{2\sigma_{b_2}^2} - \frac{(f_2 - f_{b_1})^2}{2\sigma_{b_1}^2}\right] \tag{14}$$

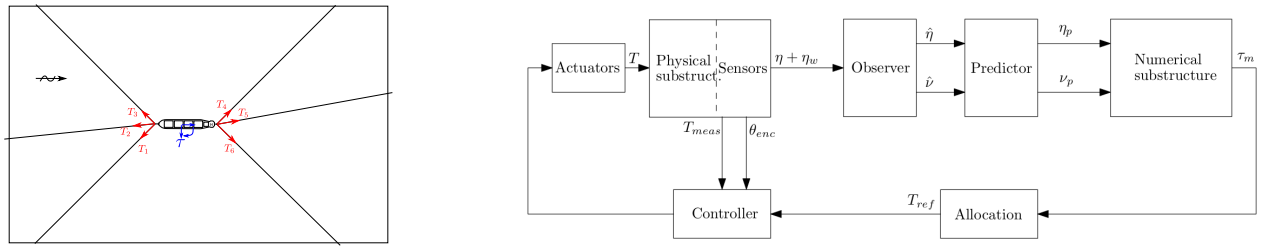

(a) (b)

Figure 2: CP model of the moored system: a) PS with actuation lines; b) block-diagram of the simulation loop.

$$Q_c = A_c \exp\left[\frac{(f_1 - f_{c_1})^2}{2\sigma_{c_1}^2} - \frac{(f_2 - f_{c_2})^2}{2\sigma_{c_2}^2}\right] + A_c \exp\left[\frac{(f_1 - f_{c_2})^2}{2\sigma_{c_2}^2} - \frac{(f_2 - f_{c_1})^2}{2\sigma_{c_1}^2}\right] \tag{15}$$

Assuming that A_a, A_b, and A_c are known, the parameter vector that fully characterizes the QTF reads

$$\boldsymbol{\theta}_F = \{f_a, \sigma_a, f_{b_1}, \sigma_{b_1}, f_{b_2}, \sigma_{b_2}, f_{c_1}, \sigma_{c_1}, f_{c_2}, \sigma_{c_2}\} \tag{16}$$

and we assume that preliminary (uncertain) estimates of $\boldsymbol{\theta}_F$ are available, for example from numerical methods.

As presented in the work of Sauder and Tahchiev [4], and shown in Figure 2a the structure under consideration is subjected to head waves in an ocean basin and kept in position using an active positioning system. The structure in its mooring is then assimilated to a single-degree-of-freedom second-order dynamical system, and its LF motions are described by

$$(m + a)\ddot{x} + d_h\dot{x} = \tau_m(x, \dot{x}) + \tau_w(t) \tag{17}$$

where x is the LF surge displacement of the floater and $\dot{x}$ its LF surge velocity. The mass term includes both floater mass m and the asymptotic value of the hydrodynamic added mass a for low frequencies; d_h is the LF damping parameter, which includes, among others, wave drift damping. $\tau_m(x, \dot{x})$ represents the restoring force of the (virtual) mooring system, which is linear w.r.t. both velocity and position. Finally, $\tau_w(t)$ is the LF load produced by a bichromatic wave with two wave components of frequencies f_1 and f_2 (with $f_1 \geq f_2$).

The numerical subsystem of the CP model coincides with $\tau_m(x, \dot{x})$ while all other terms of (17) belongs to the physical subsystem. CP testing is performed in force-control, that is, a set of actuation lines impose mooring forces τ_m to the floater, and the corresponding LF velocity $\dot{x}$ and position x feedback close the simulation loop. Figure 2b reports a block diagram of the CP setup.

Assuming bichromatic waves, the complex amplitude F of the (second-order, LF) hydrodynamic force τ_w at frequency Δf is given by the following expression

$$F = 2Q(\boldsymbol{\theta}_F, \Delta f, f_0)a_1 a_2^* \tag{18}$$

where a_1 and a_2 are the complex amplitudes of the two incoming waves. Accordingly, the complex-valued LF floater displacement X obtained at steady state can be approximated by the following scalar frequency-domain equation

$$X = H(\Delta f)F \tag{19}$$

where $H(\Delta f)$ is the transfer function of the moored system obtained from (17). The analytical expression of $H(\Delta f)$ is

$$H(\Delta f) = \frac{1}{k_m} \frac{1}{1 - \left(\frac{\Delta f}{f_n}\right)^2 + 2i\left(\zeta_h + \frac{d_m}{2\sqrt{(m+a)k_m}}\right)\frac{\Delta f}{f_n}} \tag{20}$$

where i is the imaginary unit, and k_m and d_m are the stiffness and damping coefficients of the (numerical) mooring system, respectively. The floater eigenfrequency reads

$$f_n = \frac{1}{2\pi}\sqrt{\frac{k_m}{m + a}} \tag{21}$$

Note that the total damping ratio $\zeta = \zeta_h + \zeta_m$ includes both the hydrodynamic damping ζ_h of the floater and the mooring-induced damping $d_m = 2\zeta_m\sqrt{(m + a)k_m}$. Notably, k_m and d_m are related to the numerical subsystem while m, a and ζ_h, are related to the physical subsystem. The floater mass m can be easily measured whereas the hydrodynamic added mass a and damping ζ_h need to be calibrated based on experiments.

4.2 Setting of the benchmark study

Since the CP testing campaign is virtual, the "experimental" observations are also produced numerically using the same equation utilized as the forward model. Accordingly, and in line with the format of (1), the model calibration problem is stated as follows,

$$y := |\hat{X}| = |\hat{H}(\Delta f)\hat{F}| \tag{22}$$

$$\mathcal{M}(\boldsymbol{\theta}, \mathbf{d}) := |X| = |H(\Delta f)F| \tag{23}$$

$$\epsilon \sim \mathcal{N}(0, \sigma) \tag{24}$$

where $\sigma = 0.3$ m (at full-scale) is the standard deviation of the discrepancy term. As can be appreciated from (22), the amplitude of the floater displacement is selected as experimental observation. The absolute value of the frequency-domain model of (19) is utilized both as forward model in (23) and to generate experimental observations in (22). Calibration parameters and control variables in (23) read,

$$\boldsymbol{\theta} = \{\boldsymbol{\theta}_F, a, \zeta_h\} \ , \ \mathbf{d} = \{f_0, \Delta f, k_m, d_m\} \tag{25}$$

The corresponding PDF are reported in Tables 1 and 2, respectively. The coefficients of variation (CoV) are chosen arbitrarily in this example, but should reflect expert judgment.

Table 1: Calibration parameters $\boldsymbol{\theta}$.

Parameter	Unit	Distribution	μ	CoV
f_a	Hz	Gaussian	0.090	0.05
f_{b_1}	Hz	Gaussian	0.110	0.02
f_{b_2}	Hz	Gaussian	0.120	0.02
f_{c_1}	Hz	Gaussian	0.140	0.02
f_{c_2}	Hz	Gaussian	0.150	0.02
σ_a	Hz	Gaussian	0.008	0.02
σ_{b_1}	Hz	Gaussian	0.008	0.02
σ_{b_2}	Hz	Gaussian	0.004	0.02
σ_{c_1}	Hz	Gaussian	0.004	0.02
σ_{c_2}	Hz	Gaussian	0.004	0.02
a	t	Gaussian	11770	0.10
ζ_h	–	Gaussian	0.030	0.10

Table 2: Control variables $\mathbf{d}$.

Control variable	Unit	min	max
f_0	Hz	0.050	0.200
Δf	mHz	4	13
k_m	kN/m	100	422
d_m	kNs/m	143	1284

Noteworthy, the hat symbols in (22) are introduced to emphasize that experimental observations are obtained considering the *true* values of calibration parameters, which correspond (here, for the sake of simplicity) to the mean values of Table 1. All the remaining parameters of the transfer function and the LF load in (19) are constant and reported in Table 3.

Table 3: Constant parameters.

Parameter	Unit	Value
m	t	178400
a_1	m	2
a_2	m	2
A_a	kN/m^2	150
A_b	kN/m^2	100
A_c	kN/m^2	80

In order to benchmark the accuracy of the proposed Bayesian-ED procedure, two EDs are produced and utilized to solve the calibration problem stated by (22), (23) and (24). A first ED is constructed using a Sobol' sequence [13], which is a space-filling design technique, which maximizes the coverage of the control variable space, and it is referred to as SS ED. The second ED is constructed following the procedure proposed by Huan & Marzouk [10] summarized in Section 2 and it is referred to as HM ED. Specifically, a single evaluation of the expected utility function required $n_{MC} = 1 \times 10^4$ Monte Carlo samples.

4.3 Results and discussion

The solution of the optimization problem of (6) subjected to the constraint of Table 2 took about 2 hours of elaboration using 4 CPU cores on the PRIME computer cluster of Aarhus University. Both EDs collect observations from 9 experiments, that is, $\{\boldsymbol{\mathcal{D}}, \boldsymbol{\mathcal{Y}}\} = \{\{\mathbf{d}_i, y_i\}, i \in \{1, \ldots, 9\}\}$. Corresponding samples are reported in Table 4 and overlaid to the *true* QTF in Figure 3. Note in this figure both EDs are near the bisecting line of the $f_1 - f_2$ plane. The reason is that the range of Δf is small compared to the range of f_0 (see Table 2).

Table 4: EDs computed with Huan & Marzouk procedure (HM) and with Sobol' sequence (SS).

ED	f_0 Hz	Δf mHz	k_m kN/m	d_m kNs/m	f_n [mHz]
SS	0.13	8.50	261.00	713.50	5.90
	0.09	10.75	180.50	998.75	4.90
	0.16	6.25	341.50	428.25	6.74
	0.07	9.63	381.75	1141.38	7.13
	0.14	5.13	220.75	570.88	5.42
	0.11	7.38	301.25	285.63	6.33
	0.18	11.88	140.25	856.13	4.32
	0.06	12.44	321.38	499.56	6.54
	0.13	7.94	160.38	1070.06	4.62
HM	0.17	5.61	403.01	571.84	7.33
	0.11	4.84	180.72	1056.42	4.91
	0.15	6.91	291.66	290.72	6.23
	0.15	8.71	115.81	354.30	3.93
	0.12	5.77	254.35	541.94	5.82
	0.08	4.97	188.26	660.11	5.01
	0.14	4.00	119.65	667.57	3.99
	0.18	8.78	115.78	918.91	3.93
	0.19	12.90	412.42	878.26	7.41

It is clear from Figure 3 that the HM ED tends to cluster around the lobes of the QTF whereas the SS ED is uniformly distributed along the bisecting line. Noteworthy, it is in the proximity of the QTF lobes that observations carry more information regarding calibration parameters.

Based on the HM and SS EDs, the posterior PDF of the calibration parameters were computed using *UQLab*, which is a MATLAB toolbox for uncertainty quantification developed by the Chair of Risk, Safety and Uncertainty Quantification of ETH Zurich, Switzerland [14, 15]. Firstly, the performance of HM and SS EDs are compared in terms of reduction of epistemic uncertainty in the calibration parameters, which is qualitatively

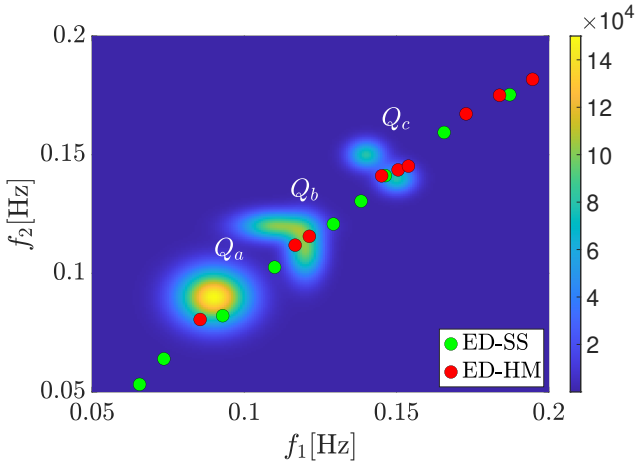

Figure 3: True QTF (in N/m^2) with both SS and HM EDs.

assessed by looking at the dispersion of the posterior PDFs. In this regard, Figures 4, 5 and 6 collect the prior and both posterior PDFs of the location parameter related for Lobes a, b and c of the QTF, respectively, namely f_a, f_{b_1}, f_{b_2}, f_{c_1} and f_{c_2}. Posterior PDFs are computed for both HM and SS EDs.

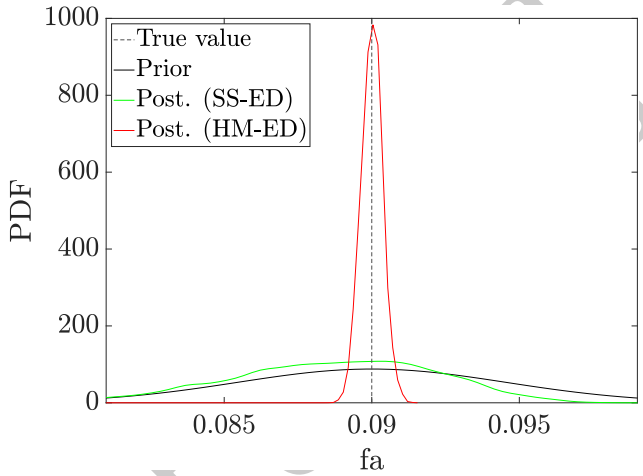

Figure 4: Prior and posterior PDFs of f_a, describing the location of lobe a of the QTF.

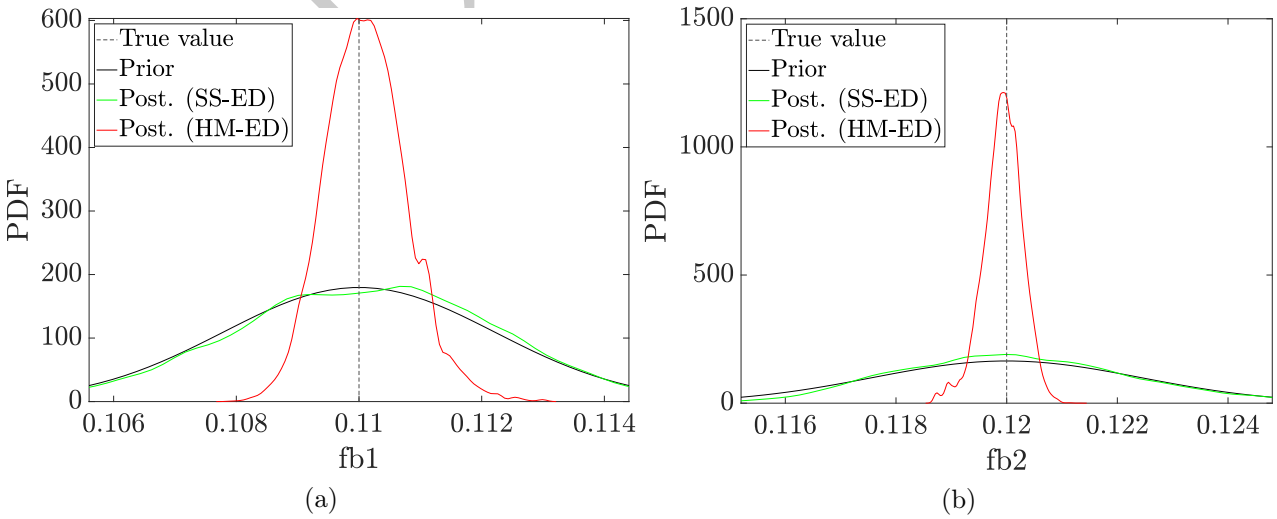

Figure 5: Prior and posterior PDFs of f_{b_1} and f_{b_2}, describing the location of lobe b of the QTF.

As can be observed from Figures 4, 5 and 6, the HM ED outperforms the SS ED in terms of reduction of uncertainty from prior to posterior PDFs. However, prior and posterior PDFs of lobe radii $\sigma_a, \sigma_{b_1}, \sigma_{b_2}, \sigma_{c_1}$ and σ_{c_2} are systematically similar for both HM and SS EDs. The same result is obtained for the floater damping ratio ζ_h and the added hydrodynamic mass a. Therefore, corresponding plots are omitted for brevity.

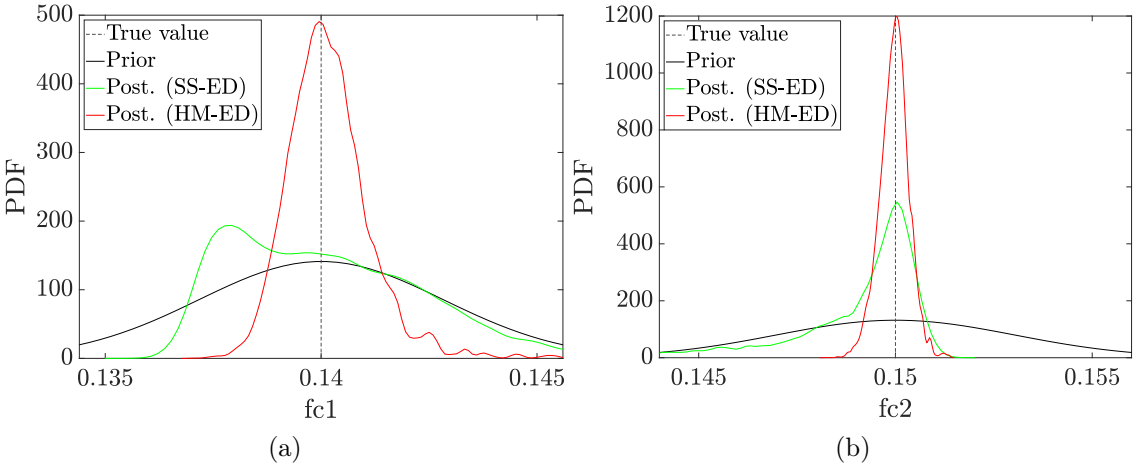

Figure 6: Prior and posterior PDFs of f_{c_1} and f_{c_2}, describing the location of lobe c of the QTF.

Notably, for none of the calibration parameters, the the SS ED outperforms the HM ED in term of reduction of epistemic uncertainty of calibration parameters. Noteworthy, (6) implies that the HM ED provides the most informative experimental design; all other solutions (including the SS ED) are sub-optimal w.r.t. the definition of the utility function (8).

Finally, in order to provide a quantitative measure of the effectiveness of the proposed procedure, for both SS and HM EDs, the Kullback-Leibler divergence from posterior to prior of the joint PDF of frequency parameters f_a, f_{b_1} f_{b_2}, f_{c_1} and f_{c_2} are computed using the nearest-neighbour method described in [16]. Numerical results are compared in Figure 7. Clearly, the HM ED is more informative than the SS ED.

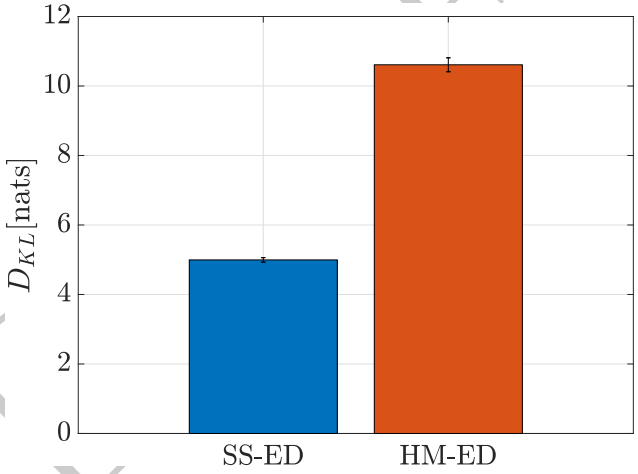

Figure 7: Kullback-Leibler divergence from posterior to prior of the joint PDF of frequency parameters f_a, f_{b_1} f_{b_2} f_{c_1} and f_{c_2}.

5 CONCLUSIONS

This paper investigates the empirical estimation of a quadratic transfer function based on a minimal set of cyber-physical tests. Bayesian experimental design is proposed to optimize the selection of the control variables for a batch of cyber-physical tests so that the expected reduction of uncertainty of the quadratic transfer function calibration parameters is maximized. Specifically, a Bayesian experimental design algorithm recently proposed by Huan & Marzouk (2013), is used.

The effectiveness of the proposed approach is demonstrated with a virtual cyber-physical testing campaign. Control variables for the experimental design include both the frequencies of bi-chromatic waves and stiffness and damping of the active mooring system. As a result, the floater transfer function can be tuned to the incoming low-frequency wave load, and the domain of the quadratic transfer function can be explored. A systematic comparison of the posterior distributions of the calibration parameters demonstrates that the experimental design computed with the proposed algorithm outperforms a reference space-filling design sequence. The outcome of this study suggests that Bayesian experimental design has significant potential for reducing the experimental

cost for calibration of hydrodynamic models.

References

[1] O. M. Faltinsen, *Sea Loads on Ships and Offshore Structures*. Cambridge Ocean Technology Series, 1993.

[2] N. Fonseca and C. T. Stansberg, "Wave Drift Forces and Low Frequency Damping on the Exwave FPSO," in *36th International Conference on Ocean, Offshore and Arctic Engineering (OMAE2017-62540)*, June 2017.

[3] C. T. Stansberg, "Linear And Nonlinear System Identification In Model Testing," in *International Conference on Non-Linear Aspects of Physical Model Tests*, (OTRC, Texas A&M University, Collage Station, Texas, USA), May 1997.

[4] T. Sauder and G. Tahchiev, "From soft mooring system to active positioning in laboratory experiments," in *Proceedings of the 39th International Conference on Ocean, Offshore and Arctic Engineering (OMAE2020-10084)*, July 2020.

[5] T. Sauder, V. Chabaud, M. Thys, E. E. Bachynski, and L. O. Sæther, "Real-time Hybrid Model Testing of a Braceless Semi-submersible Wind turbine. Part I: The Hybrid Approach," in *35th International Conference on Ocean, Offshore and Arctic Engineering (OMAE2016-54435)*, 2016.

[6] M. C. Kennedy and A. O'Hagan, "Bayesian calibration of computer models," *Journal of the Royal Statistical Society: Series B (Statistical Methodology)*, vol. 63, no. 3, pp. 425–464, 2001.

[7] J. Nagel and B. Sudret, "Spectral likelihood expansions for bayesian inference," *Journal of Computational Physics*, vol. 309, 06 2015.

[8] K. Chaloner and I. Verdinelli, "Bayesian Experimental Design: A Review," *Statistical Science*, vol. 10, pp. 273–304, Aug. 1995.

[9] E. G. Ryan, C. C. Drovandi, J. M. McGree, and A. N. Pettitt, "A Review of Modern Computational Algorithms for Bayesian Optimal Design," *International Statistical Review*, vol. 84, no. 1, pp. 128–154, 2016.

[10] X. Huan and Y. M. Marzouk, "Simulation-based optimal bayesian experimental design for nonlinear systems," *Journal of Computational Physics*, vol. 232, pp. 288–317, 2013.

[11] K. P. Murphy, *Machine learning: a probabilistic perspective*. Adaptive computation and machine learning series, Cambridge, MA: MIT Press, 2012.

[12] D. Lindley, *Bayesian Statistics, A Review*. CBMS-NSF Regional Conference Series in Applied Mathematics, Society for Industrial and Applied Mathematics, 1972.

[13] I. M. Sobol', "On the distribution of points in a cube and the approximate evaluation of integrals," *Zhurnal Vychislitel'noi Matematiki i Matematicheskoi Fiziki*, vol. 7, no. 4, pp. 784–802, 1967.

[14] S. Marelli and B. Sudret, "Uqlab: A framework for uncertainty quantification in matlab," in *The 2nd International Conference on Vulnerability and Risk Analysis and Management (ICVRAM 2014)*, pp. 2554–2563, July 2014.

[15] P.-R. Wagner, J. Nagel, S. Marelli, and B. Sudret, "UQLab user manual – Bayesian inversion for model calibration andvalidation," tech. rep., Chair of Risk, Safety and Uncertainty Quantification, ETH Zurich,Switzerland, 2019. Report # UQLab-V1.3-113.

[16] F. Perez-Cruz, "Kullback-Leibler divergence estimation of continuous distributions," in *2008 IEEE International Symposium on Information Theory*, (Toronto, ON, Canada), pp. 1666–1670, IEEE, July 2008.